Desalination and Water Treatment
www.deswater.com
doi: 10.5004/dwt.2021.26891

217 (2021) 111–126
March

Design and experimental validation of a six-effect multi-effect evaporation plant utilized in oilfield

Guangrui Cui, Mingshu Bi, Cong Liu*

School of Chemical Machinery, Dalian University of Technology, 116023, China, emails: costaliugame@mail.dlut.edu.cn (C. Liu), cuiguangrui.xuexi@foxmail.com (G. Cui), bimsh@dlut.edu.cn (M. Bi)

Received 29 June 2020; Accepted 1 December 2020

ABSTRACT

This paper focuses on desalination process of oilfield sewage and chooses multi-effect evaporation (MEE) as the main device for treatment. A mathematical model is built to describe the MEE system for sewage. It is necessary to mention that the model shows a good function of treating oilfield sewage and the fouling of the evaporator is avoided via reasonable design. Also, a six-effect experimental platform with a small capacity is designed to validate the model. Sufficient experiments are carried out and the quality of the fresh water from the system meets the requirement of oilfield reinjection. The data from the experiments are compared with the calculation and the steam loss of the model is adjusted according to vacuum degree of the evaporator. Results show that the performance ratio is 4.776 and the gained output ratio is 4.537 and the average difference between calculation and experiment is less than 4.5%.

Keywords: Multi-effect evaporation; Oilfield sewage; System design

1. Introduction

Water shortage is a global crisis that all countries have to deal with. Such a crisis is exacerbated by many factors such as population growth, industrialization and urbanization and so on. UNEP predicts that by 2025 more than 2.8 billion people in 48 countries will face water stress or scarcity conditions [1]. To make things worse, an increasing amount of sewage has been produced during the petrochemical process. As for the components of the sewage, which is listed in Table 1, chloride is a fair important component that needs treating. In many countries, desalination is an effective way that is rapidly developing. Between 2005 and 2015 alone, the desalination capacity in the world has more than doubled and this trend continues [2]. There are hundreds of methodologies for desalination and among them the methodology of distillation is widely studied as a reliable and relatively low-cost way of desalination of oilfield sewage in order to deal with a huge amount of wastewater and produce enough clean water for common use.

Together with RO and multi-stage flash, multi-effect evaporation (MEE) accounts for more than 94% of the global desalination capacity [3]. It is available for desalination of seawater and is greatly emphasized as one of the most efficient and promising methods of distillation. Studies are conducted in different directions: thermodynamic effects of different operating conditions and design parameters, anti-fouling, coupling with other equipment, low temperature multi-effect evaporation (LT-MEE), and economic calculations.

For the treatment of oilfield brine, the MEE system is chosen in this study. The heat transfer process of MEE has a relatively high heat transfer coefficient. Second, the power consumption of MEE is low, and MEE relies on the latent heat absorbed by saline sewage for water evaporation, which can reduce the sewage treatment cost. Third, MEE operates in a vacuum with relatively low

* Corresponding author.

Table 1
Composition of oilfield sewage

Name Composition/ppm	Storage tank	Softener outlet	Brine	Concentrate
HCO_3^-	335.82	425.16	927	1,010
Cl^-	2,657.15	2,834.3	31,716	13,285.75
SO_4^{2-}	58	82.3	393	290
Ca^{2+}	31.58	0	21.1	157.9
Mg^{2+}	4.94	0	2.5	24.7
Na^+ and K^+	1,832.71	2,037.39	26,799	9,163.55
Mineralization	4,920.21	5,379.97	60,135	24,601.05
Temperature/°C	89	86	80	280
Pressure/MPa	0.1	0.1	0.1	10
pH	6.8	7	6.5	7
Dissolved oxygen	0	0.05		0
SiO_2	263	82.1	350	615
Oil	5	5	10	5

operating temperature, which can avoid or slow down corrosion and fouling of the equipment. Oilfield brine has a higher degree of mineralization and more complex composition. Therefore, MEE systems are suitable for desalting oilfield brines according to its physicochemical properties.

As for oilfield sewage, many different membrane methods are developed to separate oil and high salt sewage [4]. To name a few [5–8], ceramic membranes of different materials such as α-Al_2O_3, TiO_2, ZrO_2 and mullite have been utilized in ultrafiltration, microfiltration and nanofiltration and their characteristics and performance have been tested via experiments. Thus, membrane separation using ceramic membranes could be added in MEE system as a pretreatment process, verified by the study of Muhammad et al. [9]. Also, direct contact membrane distillation (DCMD) has been studied especially for oilfield sewage desalination [10].

Calle et al. [11,12] developed a dynamic model of a solar-assisted MEE plant and discussed the influence of several parameters. After experimental validation, the numerical expectation reached a fair good agreement with the measured data. Azimibavil and Dehkordi [13] proposed a numerical methodology to investigate the dynamic simulation of MEE and studied start-up transient response of MEE and common failures during the operation. Alsehli et al. [14] presented a novel multi-effect distillation (MED) system that utilized indirect brine heating such that a medium fluid was circulated through the concentrating solar collectors and stored the energy in a charging tank. The system they proposed used land area of 92,000 m^2 for PTC at a maximum feed water mass of 67,000 metric ton of brine per day, yielding 2,200 t of distillate. The average daily performance ratio was 2, and the average specific thermal energy consumption was 1,140 kJ/kg, which showed significant improvement on the thermal efficiency.

Studies have been conducted about different ways of coupling MEE system to other devices. Based on MED/TVC system, Askari and Ameri [15,16] and Askari et al. [17] chose Linear Fresnel solar field as a thermal source, performed technical and economic analyses and also studied an MEE unit (without and with TVC) combined to an LFR solar field. Ghenai et al. [18] studied hybrid multi-effect distillation adsorption desalination (MEDAD) system powered with solar energy. They found out that with the addition of AD, the production rate of fresh water was improved by 2.68 times, achieving a 57.78% lower specific energy consumption and a 12.86% higher performance ratio (PR). Elsayed et al. [19] modeled different configurations in steady and dynamic operation and added different devices to the MED system. Farsi and Dincer [20] conducted a study on an integrated MED/membrane desalination system. The integrated system they built is able to produce 165,600 kg freshwater per day. They found out that the highest irreversible source is associated with the condenser. They also found out that with an increase in the concentration factor from 1 to 3, GOR improves 2.1%, while the transmembrane water flux in DCMD reduces about 24%, which leads to a reduction in driving force of separation in DCMD. Ali et al. [21] studied the integration of MEE and MD with different feed methods. They found that after coupling with MD, the PR of the whole system increased by 25%. Moreover, the PR of the parallel feed integrated system was up to 6.33. Guo et al. [22] developed a modified mathematical model for a spray evaporation multi-effect distillation system (SE-MED) and studied the motion and evaporation behavior of droplets in a spray-evaporation tank (SET). They found out that the SE-MED system has a high efficiency with a bleed fraction of 20% and the modified SET with a swirl air flow exhibits a much higher value of 99.86% due to the increase in particle residence time.

Kosmadakis et al. [23] considered three major points: size, number of effects and heat source temperature. In order to cover more working conditions, the number of effect varied from 3 to 30 and heat source temperature varied from 60°C to 140°C. They conclusively proposed an equation as a reference to the calculation of MED specific capital cost. Papapetrou et al. [24] assessed different factors of desalination cost such as some assumptions made during the cost calculation, the ways utilized to calculate

the water cost and so on. They also found that in certain conditions, some important aspects such as hardware cost might be neglected or considered in an inappropriate method. They finally led to a list for engineers to choose exact equations for a certain system.

This paper mainly focuses on oilfield sewage treatment (after water and oil separation). A numerical model of the whole system is established by studying the evaporator, the pre-heater, and the last effect condenser. In this paper, a forward-feed six-effect evaporation experimental platform is designed in detail. After several groups of experiments, enough data are obtained to validate the numerical model. The data are also used to study how the system performance is influenced by feed water temperature, feed water flow rate, and feed water concentration. Moreover, a method to estimate the steam loss in evaporators is proposed and validated by experiments, which further reduces the deviation of the model.

2. Theoretical calculations

2.1. Physical model

The system process can be seen in Fig. 1. Multiple evaporators are connected to form the main device of MEE. One effect means each evaporator and its operation process. The steam from each effect evaporates as a heat source into the heat transfer tubes of next effect. Meanwhile, the non-evaporated liquid flows into the next effect to continue evaporating.

The feed liquid is first transported to the final secondary steam condenser through the feed pump, which condenses the final steam produced, and at the same time achieves the purpose of liquid preheating treatment. Usually, there are four ways to feed liquid to the evaporator: forward feed, reverse feed, parallel feed and cross feed. Second, the liquid flow through the distributor is evenly distributed to the top of the heat transfer tube and forms a thin film on top of the heat transfer tube. Under its gravitational force, the liquid film drips down to the next row along the wall of the tube. After the heat transfer, the generated secondary steam diffuses to the next effective heat transfer tube as a heat source. The concentrate enters the next effective repeated spraying and falling film evaporation process until it is discharged from the last effect evaporator.

In order to release heat and condense into fresh water, the raw steam from the steam generator flows into the first effect evaporator. The secondary steam passes through the gas–liquid separator and enters the next evaporator under the effect of pressure difference, continuing to release heat. After the heat exchange between the secondary steam and the brine, temperature of the brine rises and the secondary steam is condensed. The fresh water in the first effect is the condensate from the steam generator, which needs to be refluxed back to the steam supply equipment, while the fresh water from the other effects is the product water.

2.2. Mathematical model

This study develops a mathematical model of the evaporator, the final effect condenser and the preheater of a six-effect tower evaporation system. The characteristics and assumptions are as follows:

- Boiling point elevation (BPE) is the function of concentration and temperature;
- When modeling, the concentration of sewage is taken as a key indicator;
- Calculate by using the isothermal difference method and the equal area method;

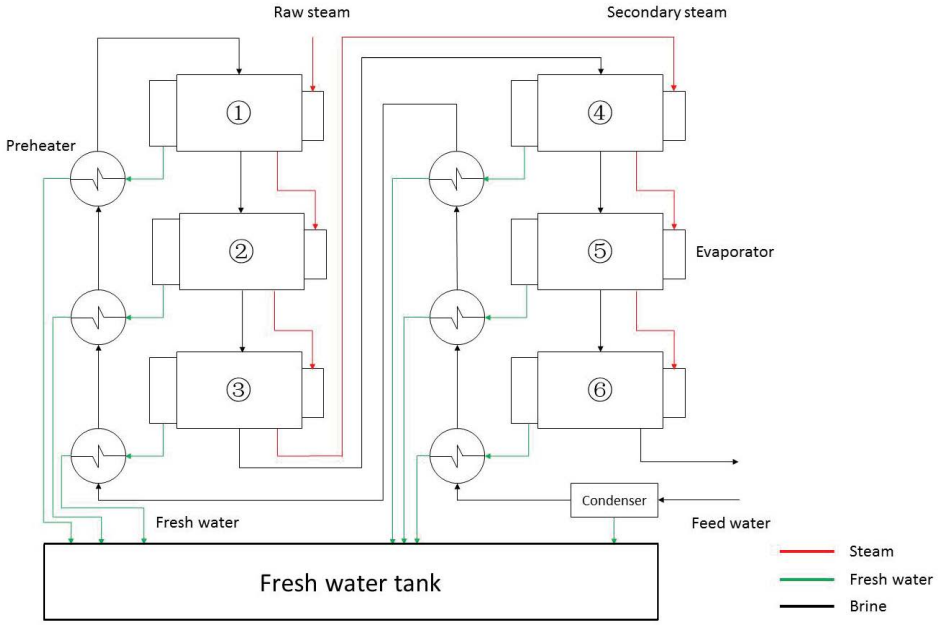

Fig. 1. System process of the six-effect distillation.

- Temperature loss caused by demister, environment, pipeline and so on is assumed to be 2°C;
- 10% of secondary steam in each effect, both generated by flashing and evaporation, is removed by vacuum pump;
- Temperature loss of raw steam is not ignorable.

2.2.1. Evaporator

First, a black-box model of the *i*-th effect evaporator is established wherein the *i*-th effect heating steam is liquefied to release heat in the heat transfer tube, which can be clearly seen in Fig. 2. Then the condensed fresh water enters the preheater to heat the feed liquid. At the same time, the concentrated liquid discharged by the *i* – 1th effect absorbs heat in the first effect, and the generated secondary steam is used as the heating steam of the *i* + 1th effect, and the remaining concentrated liquid flows into the *i* + 1th effect to be further concentrated.

The mass balance equation and energy balance equation of the *i*-th effect evaporator are as follows:

$$G_{i-1} = G_i + D_i \tag{1}$$

$$G_{i-1} \times C_{i-1} = G_i \times C_i \tag{2}$$

$$\left(0.96 \times W_i \times R_i + G_{i-1} \times \mathrm{cp}_{i-1} \times t_{i-1} - G_i \times \mathrm{cp}_i \times t_i\right) \times \eta = D_i \times r_i \tag{3}$$

Constant pressure specific heat capacity formula of the outlet liquid of the *i*-th effect evaporator is as follows:

$$X_i = 1{,}000 C_i \tag{4}$$

$$A = 4{,}206.8 - 6.6197 X_i + 1.2288 \times 10^{-2} X_i^2 \tag{5}$$

$$B = -1.1262 - 5.4178 \times 10^{-2} X_i - 2.2719 \times 10^{-4} X_i^2 \tag{6}$$

$$C = 1.2026 \times 10^{-2} - 5.3566 \times 10^{-4} X_i + 1.8906 \times 10^{-6} X_i^2 \tag{7}$$

$$D = 6.877 \times 10^{-7} - 1.1517 \times 10^{-6} X_i - 4.4268 \times 10^{-9} X_i^2 \tag{8}$$

$$\mathrm{cp}\left(X_i, t_i\right) = \left(A + B t_i + C t_i^2 + D t_i^3\right) \times 10^{-3} \tag{9}$$

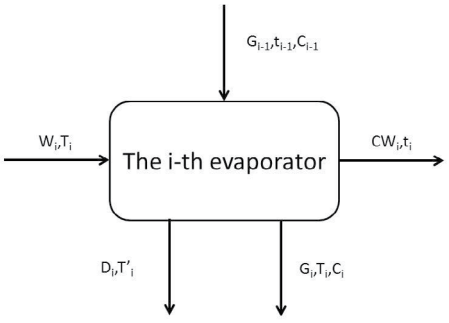

Fig. 2. Mathematical model of evaporator.

The following relationship exists between the outlet liquid temperature *t*, the heating steam temperature *T* and the secondary steam temperature *T*′ in the above formula [25]:

$$T'_{i-1} = t_i - \mathrm{BPE}_i - \Delta t' \tag{10}$$

$$T_{i+1} = T'_i - \Delta t'' \tag{11}$$

In the formula above, $\Delta t'$ refers to the temperature loss from the hydrostatic head, which can be neglected, and $\Delta t''$ refers to the temperature loss caused by the environment, pipeline, demister and so on.

The boiling-point elevation is a function of temperature and concentration and its formula is as follows [13]:

$$X_i = 100 C_i \tag{12}$$

$$A = 8.325 \times 10^{-2} + 1.883 \times 10^{-4} t_i + 4.02 \times 10^{-6} t_i^2 \tag{13}$$

$$B = -7.625 \times 10^{-4} + 9.02 \times 10^{-5} t_i - 5.2 \times 10^{-7} t_i^2 \tag{14}$$

$$C = 1.522 \times 10^{-4} - 3 \times 10^{-6} t_i - 3 \times 10^{-8} t_i^2 \tag{15}$$

$$\mathrm{BPE}\left(X_i, t_i\right) = A X_i + B X_i^2 + C X_i^3 \tag{16}$$

The heat transfer equation of the *i*-th effect evaporator is as follows [26]:

$$D_i \times r_i = K_i \times A_i \times \Delta T_i \tag{17}$$

$$\Delta T_i = T_i - t_i \tag{18}$$

K_i is mainly composed of tube condensation, tube evaporation, tube wall heat conduction and dirt resistance and the heat transfer equation is as follows:

$$K_i = \frac{1}{\frac{1}{\alpha_{i,\mathrm{in}}} + \frac{1}{\alpha_{i,\mathrm{out}}} + \frac{\delta}{\lambda} + \alpha_{i,f}} \tag{19}$$

According to the data published by Wolverine Tube [27], Nusselt et al. studied the condensing side of a horizontal cross tube, assuming zero shear in the vertical a-direction and a saturation temperature at steam pressure, and the velocity of condensate along the tube was neglected along with the effect of subcooling. The study obtained a heat transfer coefficient equation of the steam condensation inside the tube, given as follows:

$$\alpha_{i,\mathrm{in}} = 0.555 \times \left[\frac{\lambda_L^3 \rho_L \left(\rho_L - \rho_D\right) g R'_i}{\mu_L d_{\mathrm{in}} \left(T_i - t_w\right)}\right]^{1/4} \tag{20}$$

$$R'_i = R_i + \frac{3}{8} \mathrm{cp}_i \left(T_i - t_w\right) \tag{21}$$

In the equation above, R_i' refers to the corrected value of liquefaction latent heat.

An equation is derived from the study by Chun and Seban [28] in order to calculate heat transfer coefficient of liquid evaporation outside the tube:

$$\alpha_{i,\text{out}} = 0.822\frac{d_{\text{out}}}{d_{\text{in}}}\left(\frac{\lambda_i^3 g}{\nu_i^2}\right)^{1/3}\left(\frac{4\Gamma_i}{\mu_i}\right)^{-0.22} \tag{22}$$

In this model, flashing is taken into consideration after the first effect and the NEA, together with flashing temperature t_i'' and steam flow rate from flashing D_i'' are calculated with the equation developed by Miyatake et al. [29]:

$$\text{NEA}_i = \frac{33\times\left(t_{i-1}-T_i\right)^{0.55}}{T_i} \tag{23}$$

$$t_i'' = T_i + \text{NEA}_i \tag{24}$$

$$D_i'\times r_i' = G_{i-1}\times \text{cp}_{i-1}\times\left(t_{i-1}-t_i''\right) \tag{25}$$

2.2.2. Preheater

The reciprocal heat transfer between condensate and feed liquid in the heat transfer tube of the *i*-th effect evaporator not only increases the enthalpy of liquid sprayed on the wall of the heat transfer tube but also increases the proportion of heating steam used to evaporate the liquid, reduces the temperature of condensate and facilitates freshwater collection. The black box model is shown in Fig. 3.

The mass balance equation and energy balance equation of the *i*-th effect preheater are as follows:

$$CW_i = FW_i \tag{26}$$

$$G_{p,i} = G_{p,i+1} \tag{27}$$

$$Q_{p,i} = G_{p,i}\times \text{cp}_{p,i}\times t_{p,i} - G_{p,i+1}\times \text{cp}_{p,i+1}\times t_{p,i+1} = CW_i\times \text{cp}_{f,i,\text{in}} \times t_{i,\text{in}} - FW_i\times \text{cp}_{f,i,\text{out}}\times t_{i,\text{out}} + 0.04\times CW_i\times R_i \tag{28}$$

The heat transfer equation of the *i*-th effect preheater is as follows:

$$Q_{p,i} = K_{p,i}\times A_{p,i}\times\left(\text{LMTD}\right)_{p,i} \tag{29}$$

$$\left(\text{LMTD}\right)_{p,i} = \frac{\left(T_{i,\text{in}}-t_{p,i}\right)-\left(T_{i,\text{in}}-t_{p,i+1}\right)}{\ln\dfrac{T_{i,\text{in}}-t_{p,i}}{T_{i,\text{in}}-t_{p,i+1}}} \tag{30}$$

2.2.3. Last effect steam condenser

The secondary vapor generated by the final effect evaporation enters the final effect condenser (Fig. 4) as a heat source to increase the temperature of the feed liquid. At the same time, the feed liquid acts as a cold source to make the final effect secondary vapor phase change and condense. One part of the liquid flows into the device, and the other part is discharged.

The mass balance equation and energy balance equation of the last effect condenser are as follows:

$$F_{\text{in}} = F_{\text{out}} \tag{31}$$

$$Q_{c,n} = 0.96\times D_n\times r_i = F_{\text{in}}\times\left(\text{cp}_{\text{out}}\times t_{\text{out}} - \text{cp}_{\text{in}}\times t_{\text{in}}\right) \tag{32}$$

The heat transfer equation of the last effect condenser is as follows:

$$Q_c = K_c\times A_c\times\left(\text{LMTD}\right)_c \tag{33}$$

2.3. Index of system performance

2.3.1. Total freshwater yield

Total freshwater yield D is the sum of condensate flow rate in heat transfer tubes of all effective evaporators except the first effect evaporator, formula of which is:

$$D = \sum_i^n D_i = D_1 + D_2 + \ldots + D_n \tag{34}$$

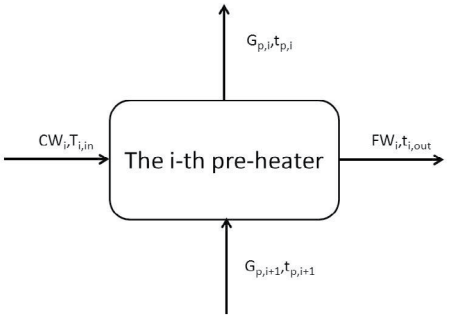

Fig. 3. Mathematical model of preheater.

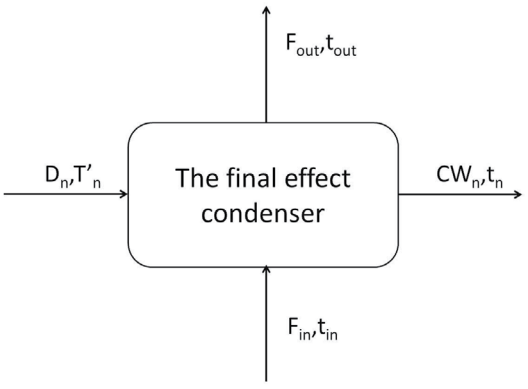

Fig. 4. Mathematical model of last effect condenser.

This equation can be derived from Eqs. (1) and (2):

$$D = G_0 \times \left(1 - \frac{C_0}{C_n}\right) \tag{35}$$

And obviously:

$$D = \sum_i^n D_i = G_0 \times \left(1 - \frac{C_0}{C_n}\right) \tag{36}$$

2.3.2. Gained output ratio

Gained output ratio (GOR) refers to the mass of fresh water produced by consuming unit mass steam; the formula is as follows:

$$\text{GOR} = \frac{D}{W_1} \tag{37}$$

2.3.3. Performance ratio

The performance ratio (PR) is the ratio of the heat consumed by all the distillate to the heat provided by the raw steam. The PR is calculated as follows:

$$\text{PR} = \frac{\sum_i^n D_i r_i}{W_0 r_0} \tag{38}$$

3. Design of six-effect distillation experimental system

3.1. Design of system parameters

3.1.1. Initial values

The MEE desalination system established in this paper is a small six-effect MEE experimental system with tower structure, downstream feed, which combines secondary steam condensate preheating and end-effect condenser as well. Referring to the water quality of oilfield wastewater given in Table 1, the initial design parameters of MEE system for effective deep desalination of oilfield wastewater are listed in Table 2.

Table 2
Design parameter table of six-effect MEE system

Parameter	Value
Number of effect n	6
System capacity G_0, kg/h	500
Brine initial temperature t_0, °C	40
Brine initial concentration C_0, %	2
Concentration ratio CR	2
Heating steam temperature T_1, °C	120
Last effect secondary steam temperature T'_6, °C	45
First effect preheater cold source outlet temperature, °C	63
Equipment heat utilization rate η, %	98

3.1.2. Parameter solving

Taking advantage of mathematical models built in Chapter 2.3, parameters can be solved, which are listed as follows:

- Outlet low rate, temperature, and concentration of the brine in each effect evaporator;
- Flow rate and temperature of secondary steam in each effect evaporator;
- Heat transfer area of each evaporator, preheater, and condenser;
- Inlet and outlet temperature and flow rate of each preheater;
- Inlet and outlet temperature and flow rate of the cold source and heat source of the condenser;
- Heat transfer area required for each preheater and condenser.

3.1.3. Calculation process

3.1.3.1. Evaporator

The calculation method utilized in this paper combines the equal temperature difference method with the equal area method. The equal temperature difference method is a method for solving various parameters of the evaporator in the case where the heat transfer temperature differences of every effect are equal. The equal area method refers to a calculation method under the condition that the heat transfer areas of every effect are equal. The calculation process is showed in Fig. 5. With known parameter inputs, the theoretical GOR is obtained from the empirical formula. Next, starting with the first effect evaporator, the various parameters of the evaporator are calculated from the evaporator mass balance equation, the energy balance equation and the heat transfer equation. In the solution process, it is necessary to determine the error between the theoretical GOR and the actual GOR, as well as the heat transfer area error of each effect. If the deviation is within the allowable range, the result is output directly; otherwise, the calculation needs to be repeated until the allowable requirement is reached.

3.1.3.2. Preheater and condenser

The calculation process is shown in Fig. 6. The solving process is according to the known parameters and the mathematical model established, the parameters are solved in the order from the first-effect preheater to the sixth-effect, and the cold source inlet temperature of the sixth-effect preheater is taken as the cold source outlet temperature of the condenser, and finally the condenser output parameters are found from the energy equation and heat transfer equation.

3.1.4. Calculation results

3.1.4.1. Evaporator

Based on Eqs. (10)–(12), average heat transfer coefficients of each effect evaporator are obtained and process parameters are listed in Table 3.

3.1.4.2. Preheater

The brazed plate heat exchanger is used as the preheater and condenser of the six-effect system. When calculating, the heat transfer coefficient is taken as 2.5 kW/(m² K) and the process parameters are shown in Table 4.

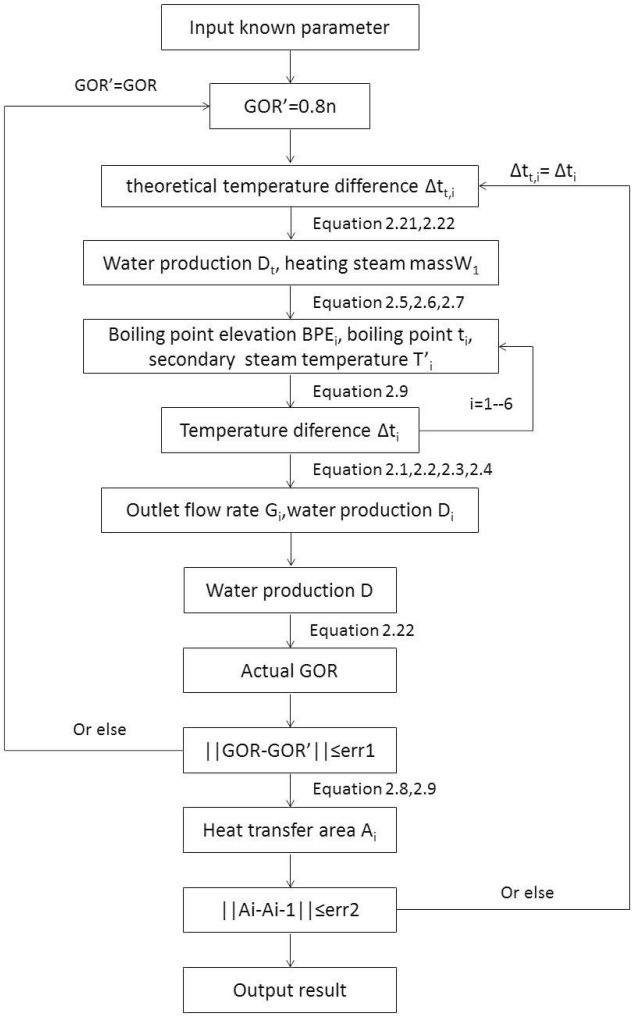

Fig. 5. Calculating process of evaporator.

For the specifications, processing cost and heat transfer efficiency of the brazed plate heat exchanger, the heat transfer area of the second, third and fourth effect preheaters is 0.2 m², while heat transfer area of the first and fifth effects are 0.3 m² and the sixth effect is 0.4 m². Plus, the heat transfer area of the condenser is taken as 0.5 m².

3.2. Design of system process

In this study, the vertical tower connection was chosen as the connection method because it is more compact, has lower operating costs, and provides better liquid film coverage. The entire experimental platform, shown in Fig. 7, consists of a heated steam side, an evaporation side, a water supply circulation side, and a non-condensing side.

3.2.1. Design of heating steam side

The heating steam system consists of a steam boiler, a boiler feed tank and a steam-metering tank. Water flows

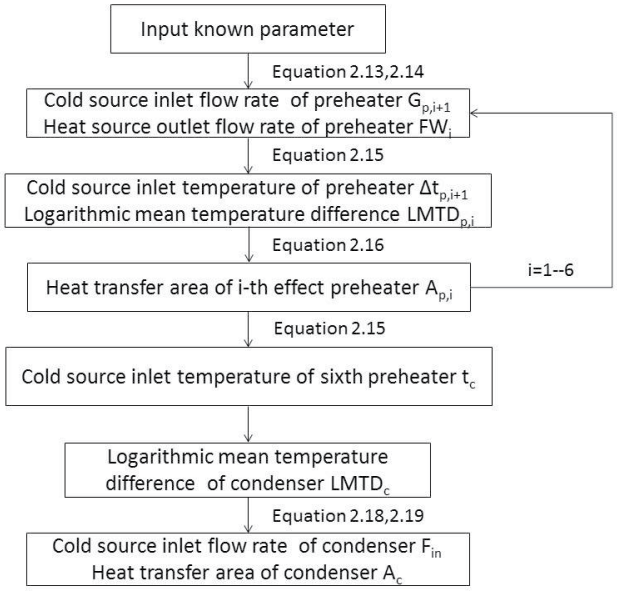

Fig. 6. Calculating process of preheater and condenser.

Table 3
Calculation parameter table of six-effect evaporator

Parameter	Effect					
	1	2	3	4	5	6
Boiling point t_i, °C	88.54	83.66	74.03	63.73	53.56	43.62
Secondary steam flow rate D_i, kg/h	31.14	33.87	39.70	44.90	48.85	51.55
Secondary steam temperature T'_i, °C	88.04	83.16	73.53	63.23	53.06	43.12
Outlet flow rate G_i, kg/h	468.86	434.99	395.29	350.40	301.55	250.00
Outlet concentration C_i, %	1.066	1.149	1.265	1.427	1.658	2.000
Heat transfer area A_i, m²	1.553	1.557	1.555	1.553	1.553	1.551
Heating steam flow rate W_i, kg/h	56.77					
Gained output ratio	4.40					

Table 4
Calculation parameter table of preheater

Effect	Cold source				Heat source				Heat transfer area
	Inlet		Outlet		Inlet		Outlet		
	Flow rate	Temperature	Flow rate	Temperature	Flow rate	Temperature	Flow rate	Temperature	
1	500	57	500	63	56.77	100	56.77	69	0.230
2		54		57	29.51	90.5	29.51	62.7	0.138
3		51		54	35.60	81.5	35.60	57.7	0.173
4		48		51	10.78	72.5	40.78	56.6	0.181
5		45		48	48.02	63.5	48.02	52	0.240
6		42		45	48.34	54	48.34	46.4	0.394
Condenser	12,600	20		42	50.75	45.5(g)	50.75	45.5(l)	4.742

Unit of area is m^2; unit of temperature is °C and unit of flow rate is kg/h.

Fig. 7. Design of experimental platform.

into the boiler from the feed tank. The steam produced by the boiler serves as the heating steam for the first effect evaporator, and the condensed liquid flows out of the evaporator and into the first effect preheater. After the completion of the heat exchange process, the condensate of heated steam flows into the steam-metering tank, which measures the flow rate of the steam boiler. When the steam boiler is short of water, the liquid in the water tank returns to the supply tank for recycling. The system flow is shown in Fig. 8.

3.2.2. Design of water supply circulation side

The water supply circulation side is divided into three parts: the feed liquid side, the product water side, and the concentrate side.

3.2.2.1. Feed liquid side

In the operation of the equipment, the liquid from the condenser is divided into two streams of feed liquid and one stream of outflow liquid. If the outflow liquid is discharged directly into the environment, it is bound to be wasted. In the design of the structure, the collection of this part of the condensate should be paid attention to, in order to achieve the purpose of reuse. The inlet side adopts a vertical installation structure, with the upper and lower tanks of the structure connected to feed pumps and flow meters, and the upper tank is responsible for collecting and discharging the condensate and providing raw materials for the lower tank.

3.2.2.2. Product water side

The fresh water produced in each effect needs to be collected in a fresh water tank. However, due to the height

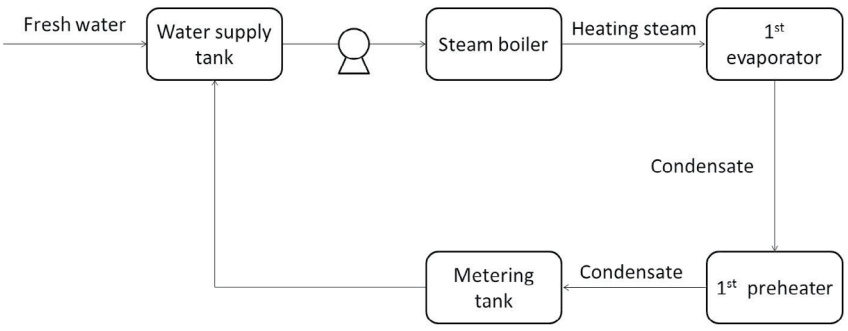

Fig. 8. Process of steam heating system.

of the tank, the pressure in the tank is greater than the pressure in each effect evaporator, which is hard for the direct collection of fresh water. In addition, by injecting the product water from each effect into the water tank, the fresh water produced by each effect evaporator cannot be measured, which is not conducive to the performance evaluation of the device. Therefore, a freshwater buffer tank was added between the device and the freshwater tank. The non-condensable gas was removed from each evaporator and the freshwater buffer tank when the device was started, and the vacuum level of the freshwater buffer tank was adjusted to be higher than the vacuum level of the other evaporators. Also, the freshwater buffer tank is located below each effect evaporator so the freshwater automatically flows into the buffer tank due to the gravity of the freshwater and the pressure difference between the evaporator and the buffer tank. At the end of the experiment, the buffer tank drain valve is opened and the freshwater in the buffer tank is drained into the freshwater tank.

3.2.2.3. Concentrate side

The concentration side is mainly composed of the last effect evaporator, self-priming pump and concentration water tank. As the experiment progresses, the liquid level in the last effect evaporator is increasing. If the heat transfer tubes are immersed in the brine, the evaporation performance will be affected. It is, therefore, necessary to continuously discharge the brine accumulated inside the device. The liquid level is observed through a window on the evaporator, and when the liquid approaches the heat transfer tube, the self-priming is turned on to discharge the concentrated liquid.

3.2.3. Design of non-condensing side

Prior to system operation, the system should be pumped out to ensure that the liquid evaporates under vacuum. In addition, during the operation of the system, with the generation of secondary vapors and the rise of the liquid level of the device, the pressure in the evaporator tank will change, so it is necessary to pump out the non-condensable gas to maintain the vacuum level of the system. Considering that a portion of the vapor in the evaporator will be withdrawn during vacuum pumping, emulsification will inevitably occur if a vacuum pump with oil as the working medium is selected. Therefore, the water-ring vacuum pump is used in this experimental system. Nevertheless, the performance of the water-ring vacuum pump is reduced due to the high temperature of the water vapor pumped by the water-ring vacuum pump. Therefore, a plate heat exchanger is added between the device and the vacuum pump, as shown in Fig. 9.

When the system is pumping the non-condensing gas, the feed water is used as a cold source to exchange heat with the extracted water vapor. On the one hand, the feed water whose temperature rises is returned to the feed water tank; on the other hand, the condensed water vapor enters the vacuum pump as a working medium. The addition of the plate heat exchanger can maintain the safe and efficient operation of the vacuum pump, ensure the vacuum degree of the device, and increase the temperature of the feed liquid.

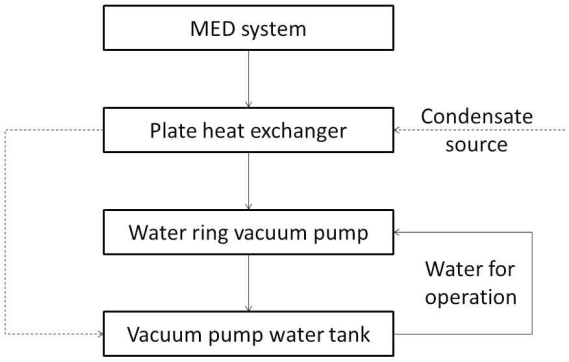

Fig. 9. Process of vacuum system.

3.3. Design of evaporator structure

The evaporator is the main part of the system, as can be seen in Fig. 7, which is composed of the left pipe box, the box and the right pipe box. There is a window at the front of the left pipe box for observing the steam condensate level, and a condensate outlet at the bottom; there is a level window at the front of the evaporator box, and the evacuation interface and liquid distribution interface are arranged at the back end, with a vacuum gauge at the top; the thermal resistance is connected with the secondary steam outlet, with a concentrated liquid outlet at the bottom; and there is a heating steam inlet at the right end of the right pipe box. The key to the operation of the system is the corrosion resistance of the equipment, the sealing and the formation of film on the outside of the heat exchanger tube. The following three aspects are introduced in terms of equipment materials, evaporator structure and distributor design:

3.3.1. Device material

The evaporator bodies and the fresh water storage tanks are all made of ultra-low carbon austenitic 316-L stainless steel as the shell material. This is due to the high salt content of oilfield wastewater, especially the high concentration of chloride ions, which puts forward a high demand on the corrosion resistance of the equipment. In terms of heat transfer tube, aluminum brass HAI77-2 is chosen as a material due to the relatively good heat transfer performance and outstanding corrosion resistance.

3.3.2. Structure of evaporator

The secondary steam produced by the previous effect enters the steam line from the right tube box, and as it flows through the tank heat transfer tube, the heat is transferred to the brine, and the condensate flows along the straight tube into the left tube box. The secondary steam in the tank flows from the upper steam line into the next effective heat transfer tube; the unevaporated brine continues to flow out through the lower tank tube. This structural design reduces the heat loss caused by local friction, and the node parameters are closer to the design value. Such design further reduces the device volume while ensuring low fluid resistance.

3.3.3. Distributors

At present, there are many studies on the determination of spray hole spacing. According to Bellman and Pennington's [30] research, the fixed length between adjacent droplets or liquid columns tends to the Taylor's inequality in the process of the droplet and columnar film falling. For non-viscous and incompressible liquids, the critical and safe Taylor wavelength equation is as follows:

$$\lambda_c = 2\pi \times \left(\frac{\sigma}{g \times (\rho - \rho_c)} \right)^{1/2} \tag{39}$$

$$\lambda_d = \sqrt{3}\lambda_c \tag{40}$$

Lienhard and Wong [31] obtained the separation distance equation by studying the separation of vapor bubbles in horizontal transverse tube thin-film evaporation:

$$\lambda_c = 2\pi / \left(g \times \frac{\rho - \rho_c}{\sigma} + 2/d^2 \right)^{1/2} \tag{41}$$

$$\lambda_d = \sqrt{3}\lambda_c \tag{42}$$

Marno-moalem et al. [32] studied the relationship between spraying quantity, tube diameter, tube spacing, and wavelength, and drew the conclusion that liquid wavelength is inversely proportional to spray amount, and is directly proportional to the tube spacing and tube diameter. According to the film columnar falling model established by Ganic and Roppo [33], a conclusion is obtained that the spray amount and the distance between the tubes are independent of λ, and λ is smaller than the wavelength solved by Taylor's inequality.

The design of a good distributor is the key to the smooth evaporation of falling film. There is no bubble in the evaporator during the operation of the device, so the spacing of the holes can be calculated by referring to the equation derived from the study by Yang and Shen [34]:

$$\lambda = 2\pi \times \left(\frac{n\sigma}{\rho g} \right)^{1/2} \tag{43}$$

When the liquid film covering the horizontal tube is thinner, it is suggested that n take 2, while for the thicker liquid film, it is suggested that n take 3. By calculating Eq. (43), the distance between two adjacent holes is calculated to be 21.8 mm. For easy processing, the distance between holes is 20 mm.

The design parameters of the distributor are as follows: 10 tubes made from 316 L stainless steel with diameter of 14 × 1 and length of 570 mm, each spray tube has 26 spray holes with diameter of 2.0 mm at the bottom, and the two outermost spray tubes have spray holes with inward deviation of 30 degrees, which is more conducive to liquid film formation on the wall of the tube.

3.4. Cost of MEE system

3.4.1. Capital cost

The specific capital cost of the system is calculated in detail and shown in Table 5. It can be seen that the specific capital cost is 31.93% lower than 4,142.7 USD/(m^3/d), which is calculated by equation from the study by Kosmadakis et al. [23].

3.4.2. Operation cost

The operation cost of the MEE system includes electricity cost, thermal cost, labor cost, chemical cost, maintenance cost, etc. The specific cost of each cost is referenced to existing research and the operating costs of the established MEE system are listed in Table 6.

4. Results and discussion

A series of experiments were conducted using the six-effect MEE system. The whole system takes an average of 2.42 h to reach the steady state. At steady state, the mineralogy of the freshwater produced by the system was tested to be 9–24 ppm, which is in line with the oilfield re-injection water quality requirements. The actual salinity is lower than the tested value, considering the influence of impurities in the system itself. Under the design condition, the PR is 4.776 and the GOR is 4.537. These results also validate the feasibility of the experimental platform.

Three main parameters, such as concentration, inlet temperature and inlet flow rate, were studied by analyzing the experimental and calculation results. In addition, the performance of the system is mainly expressed via the PR, GOR, and the amount of fresh water. Below are the experimental and calculation results and the results are studied from the perspective of the three parameters.

4.1. Influence of concentration

The results of the experiments and calculations are shown in Fig. 10. The concentration of feed water has little effect on the freshwater flow rate, so much so that a 12% increase in concentration results in only a 10% increase in freshwater yield. The reason for this relative increase may be that the increase in the boiling point of the brine reduces the temperature difference between the effects and increases the

Table 5
Capital cost of MEE system

Equipment	Number	Cost/USD
Evaporator	6	15,900
Preheater	6	9,750
Pump	5	7,830
Water tank	8	2,400
Pipeline	N/A	510
Capital cost		33,840
Specific capital cost USD/(m^3/d)		2,820

Table 6
Operation cost of MEE system

Category	Specific cost	Amount	Cost USD/y
Electricity cost	0.05 USD/kWh	3.85 kW	1,686.3
Thermal cost (steam)	0.007 USD/kg	50 kg/h	3,066
Labor cost	0.03 USD/m^3	12 m^3/d	131.4
Chemical cost	0.03 USD/m^3	12 m^3/d	131.4
Maintenance cost	3% of capital cost		1,015.2
Total cost USD/y			6,030.3

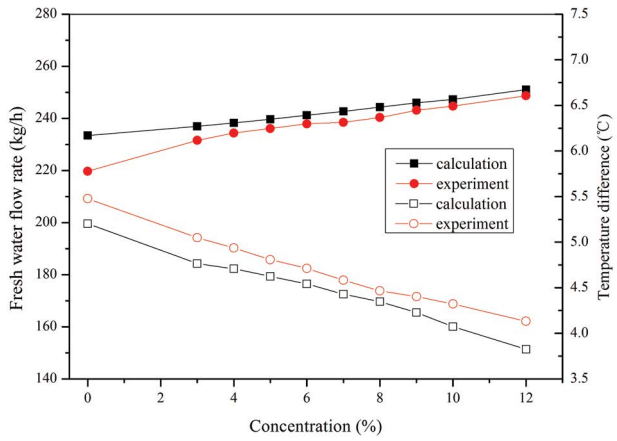

Fig. 10. Influence of concentration.

heat transfer rate. This change is linear with concentration, as can also be seen in the figure.

For oilfield brine, the salt concentration may not remain constant. Variations in concentration can affect the physical properties of the brine. However, for this system, it is easy to see from the figure that a change in feed water concentration in a small range (4%–10%) will not have a large effect on the system. The reasons for this phenomenon are as follows: (1) For the oilfield brine with sodium chloride as the main component, the properties such as the viscosity of the solution do not change greatly with concentration, thus not affecting the stability of the liquid film. (2) With the change of concentration, the change of BPE is not obvious. This is reflected in the small change in temperature difference between effects (within 0.5°C). (3) As the concentration changes have less effect on the working pressure, the amount of secondary vapor in each effect is more stable, thus ensuring a more stable heat source for the next effects. In this case, the system performance is thus not greatly affected.

4.2. Influence of feed water temperature

The performance of the six-effect MEE system with different feed water temperatures can be seen in Fig. 11, where Figs. 11a and b are, respectively, 70°C and 75°C.

For different feed water temperatures, freshwater yield in effects from the first to the sixth shows a similar tendency. Freshwater flow rate declines from the first effect to the sixth effect due to the gradual loss of heat in the whole system. Besides, it is easy to find out that in the first effect, the calculation value is a bit lower than the experiment value and the deviation gradually goes up from effect 2 to 6. It is because of the existence of a vacuum degree in each effect. In the first effect, the vacuum degree is relatively low (around 0.02 MPa), which leads to a relatively small steam loss caused by the vacuum pump. In the mathematic model, 10% of secondary steam could be too much and such analysis is done in order to make the model more accurate. As for effect 5 and effect 6, the vacuum is much higher than the former effects and more steam is pumped out. In such a case, the loss of steam (10%) could be underestimated.

This study repeats the experiment with different feed water flow rates. It is necessary to mention that the percentage of the loss does not change with the capacity because the bigger capacity requires more evaporator volume and the same vacuum degree leads to the same loss. At different feed water flow rates, the vacuum level of each effect remains essentially constant, and the heat loss per effect may vary, but this phenomenon persists, suggesting that it is independent of the heat loss within the effect. Thus, the deviation is mainly caused by the vacuum degree.

As for the percentage, a new assumption about the loss of secondary steam is made as shown in Table 7.

After the change of loss percentage, the results from 65°C to 90°C are listed in Fig. 12. In this figure, the model becomes more accurate and the average deviation is less than 4.2%, which validates the loss percentage proposed before. The later results take the new loss percentage in the calculation.

The performance of the whole system is depicted in Fig. 13. In the figure, the PR (a) and GOR (b) increase while the temperature of feed water goes up and the deviation, less than 5%, is quite small, which to some extent validates the model built in Chapters 2.2.1, 2.2.2 and 2.2.3. The explanation for this trend in the figure is as follows: (1) The higher feed water temperature decreases the temperature difference between the cold source and heat source in the first effect evaporator, which in turn increases the heat transfer coefficient of the evaporator, which not only ensures full utilization of raw steam but also improves the boiling state of brine in the evaporator. (2) The higher feed water temperature increases the evaporation capacity of the first effect evaporator under the same flow of raw steam. For every 10°C increase in the temperature, each effect produces about 6%–10% more secondary steam. More secondary steam not only raises the GOR and PR, but

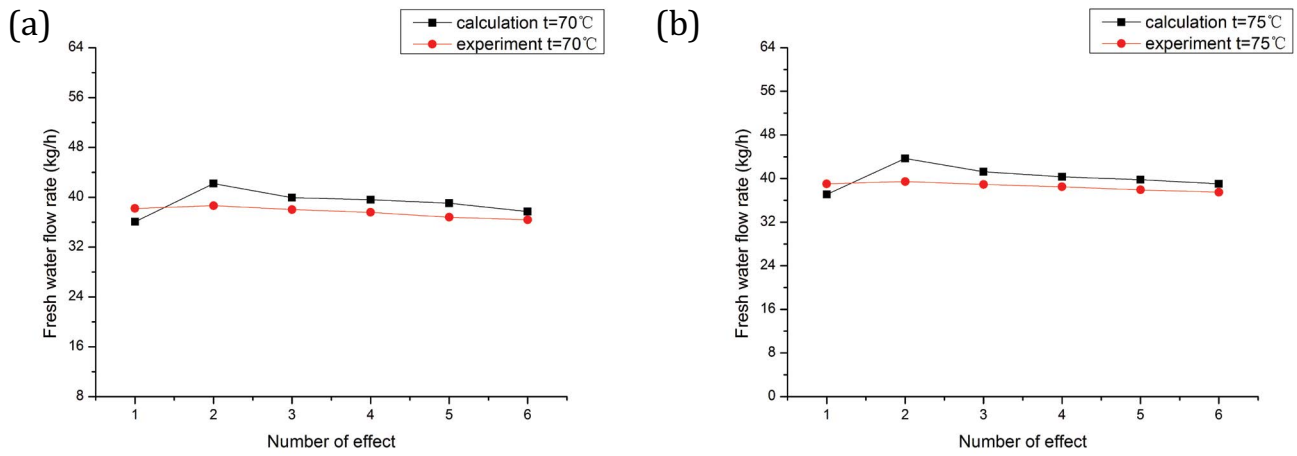

Fig. 11. Different feed water temperature.

Table 7
Loss percentages according to vacuum degree

Vacuum degree/MPa	0–0.02	0.02–0.04	0.04–0.06	0.06–0.08	0.08–0.10
Loss percentage/%	6.5	8.5	10.5	12	13

also proportionally strengthens the turbulence of steam in the pipe bundle, thus improving the heat transfer effect. (3) The increase in feed water temperature also raises the operating temperature of the evaporator accordingly. The temperature of the secondary steam in each effect is increased, which ensures the increase of the evaporation capacity of the second to sixth effect. Thus, the performance of the system is also improved. (4) Due to the increase of the secondary steam flow and temperature of each effect, the heating capacity of the preheating part of the system is enhanced, which also has a positive impact on the stability of the MEE system. Therefore, an appropriate increase in the inlet flow temperature is beneficial to the overall system performance.

4.3. Influence of flow rate of feed water

A third series of experiments are carried out to find out how the flow rate of feed water affects the performance of both single effect and the whole system. Results of different effects in MEE are illustrated in Fig. 14.

A similar tendency of freshwater flow rate is shown in results so in Fig. 14, two figures where feed water flow rates of 400 kg/h (a) and 525 kg/h (b) are picked out to present all the experiments. Plus, three different feed water flow rates are put together to show the difference. Fig. 15 shows how different flow rate (from 400 to 600 kg/h) influences the performance of the MEE system. In these figures, it is clear that a large difference in feed water flow rate results in an even larger declination in freshwater yield in Fig. 14c. Plus, the decrease of freshwater production is relatively small in the former three effects, but is particularly noticeable in the latter three effects. In this study, the flow rate of the raw steam in the first effect evaporator is fixed, so under the same feed water temperature, the evaporation capacity of the first effect evaporator is also relatively fixed. When the feed water flow rate is relatively small, the liquid film outside the tube is thin and the flow rate is relatively slow, so the fresh water flow rate of each effect will be slightly larger. After the flow rate of the feed water becomes larger (600 kg/h), compared with the experiment with low inlet flow, the liquid film outside the tube is thickened, the flow rate is accelerated, the heat exchange in the evaporator becomes worse, and the heat loss during the flow between the effects becomes larger. As a result, there is a slight decrease in the fresh water flow rate of the first few effect evaporators. However, in the last few effect evaporators, since the flow of concentrated brine is still at a large state, the heat loss is correspondingly large, the secondary steam for heating is even less, which leads to a significant drop of fresh water flow rate in the last few effects. If the yield drop is to be reduced, additional insulation for the latter effect evaporators is needed to reduce heat loss. In this way, the secondary steam flow rate of the latter effects can be guaranteed. In addition, it can be considered in future studies to inject an external heat source, such as the product steam of the TVC, into the latter effects in order to guarantee the performance of the latter effect evaporators.

The PR and GOR of the system fell gradually as the inlet flow rate increased. As the inlet flow rate changes from 400 to 600 kg/h, both indicators fall by more than 10%. The process of decline is nearly linear, indicating that the essential factors affecting PR and GOR in this process are linear factors such as brine flow rate and liquid film thickness.

When the feed water flow rate is low, the flow is relatively slower. Slower brine flow leads to a better heat

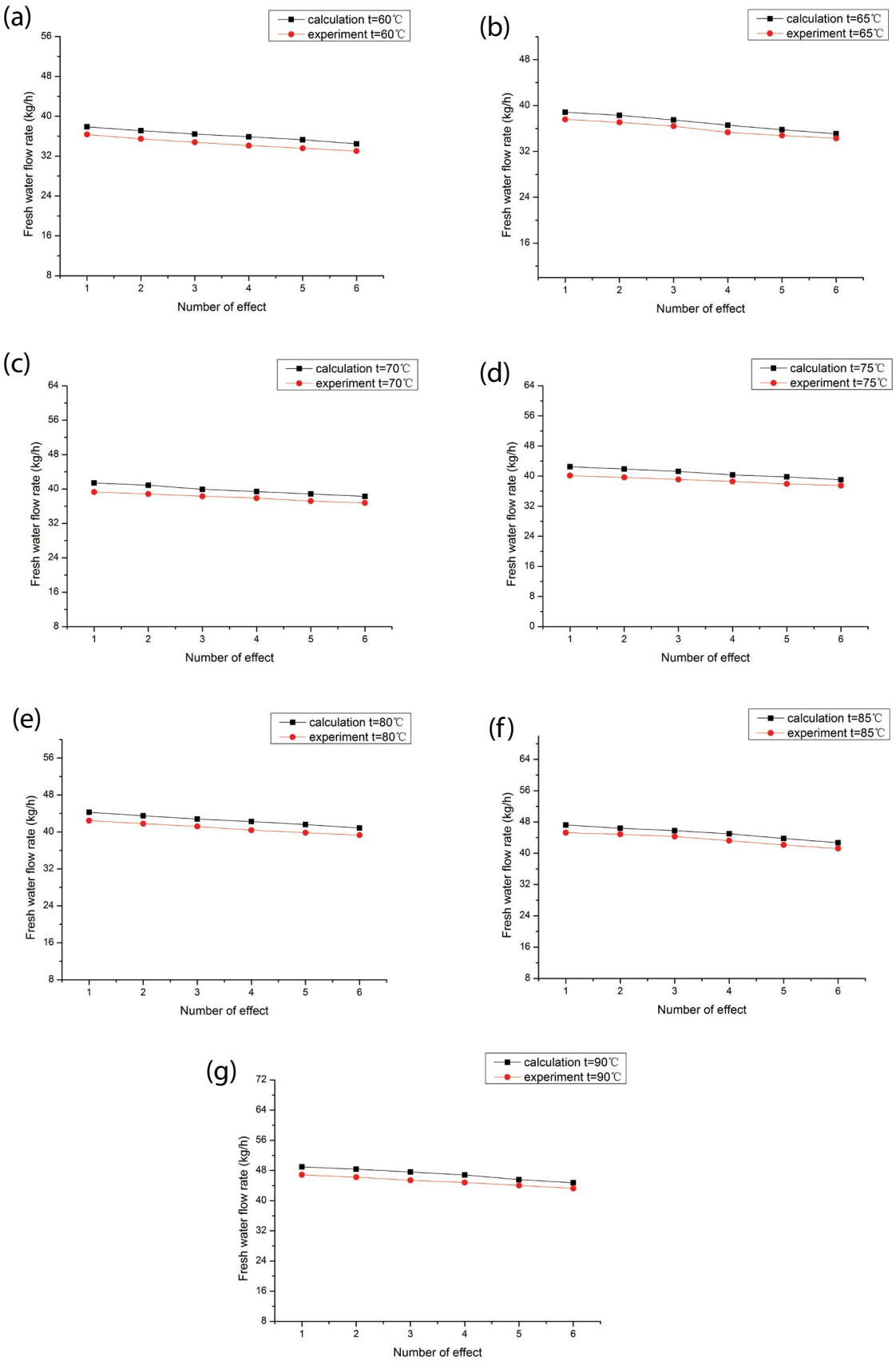

Fig. 12. Different feed water temperature.

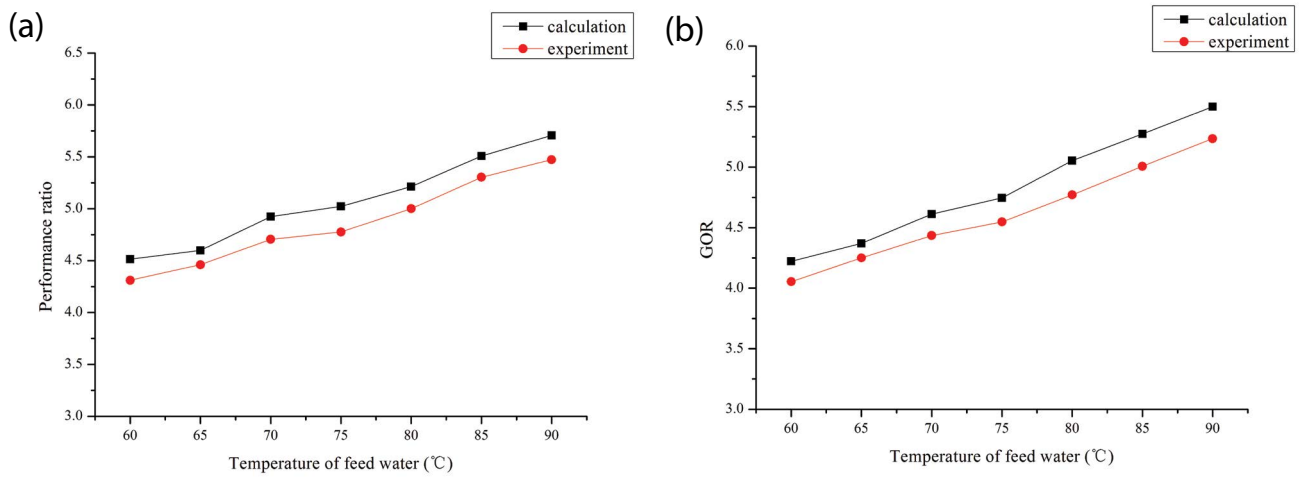

Fig. 13. System performance in different feed water temperature.

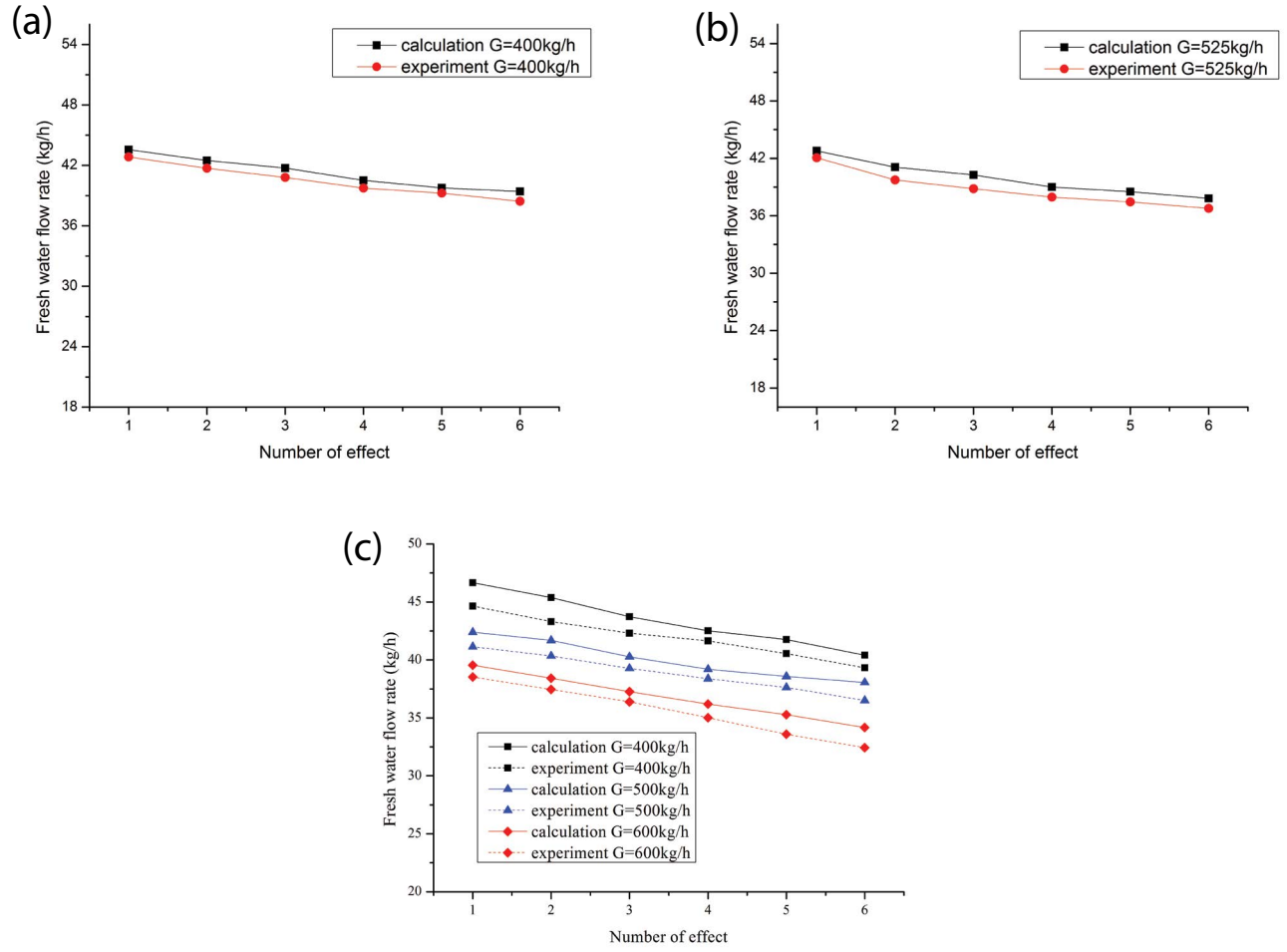

Fig. 14. Different feed water flow rate.

exchange with the steam and thus more secondary steam can be produced. When the flow rate is kept above 400 kg/h, the liquid film in each effective evaporator is more stable, which can ensure full utilization of the heat source. When the flow rate is 400 kg/h, steam starts to flow out from the hot end outlet of each effect. This is due to the increased amount of secondary steam, flowing faster in the evaporator tube and thus a small amount of steam in time for heat exchange will flow out of the evaporator. If the inlet water flow rate is further reduced, dry burning will occur

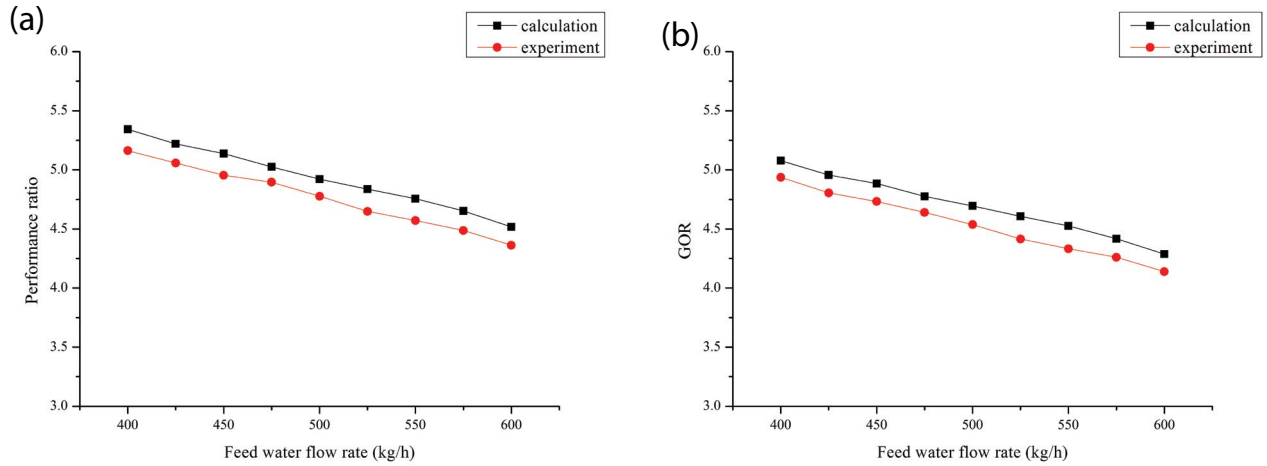

Fig. 15. System performance in different feed water flow rate.

in the evaporator, and more raw steam will flow out of the first effect evaporator in the gaseous state. The amount of secondary steam in the first effect will also be reduced, thus adversely affecting the performance of the next five evaporators.

It should also be noted in the experiment that at a flow rate of 600 kg/h, a certain amount of brine accumulation occurred for each effect. As a liquid seal, the existence of this brine is understandable, but the brine level in the evaporator in the latter effects has been close to the bottom row of evaporation tube, which indicates that a large number of brine flow to the next effect when the flow rate is too large to evaporate in time. If the inlet flow rate continues to increase, the water may not pass the evaporation tube in the evaporator in the last few effects at steady state. At that time, the PR and GOR of the system will drop sharply. In turn, it is necessary to ensure that the inlet flow rate of the system is not higher than 600 kg/h, so as not to seriously affect the working effect of the system.

Through experiments, it is found that the MEE system built in this study allows a feed flow rate of 400–600 kg/h with a fluctuation range of ±20% of the design conditions. In this range, the system performance is fairly good. Compared with adjusting the inlet temperature alone, the feed water flow rate affects more operating parameters and is, therefore, more difficult to analyze.

5. Conclusions

In this paper, a six-effect MEE system is established numerically and experimentally aiming to deal with dense brine from oilfield sewage.

- Via reasonable assumption, a mathematical model of the whole system is built, which includes an evaporator, preheater, and condenser. Also, a six-effect MEE system with a small capacity is built, in order to validate the mathematical model and verify the feasibility of the application of MEE in Chinese oilfield sewage desalination. The PR is 4.776 and the GOR is 4.537. The idea and process of design of MEE have a very good guiding significance for the future oilfield brine treatment.
- In this study, a rather accurate ratio of steam loss is proposed according to the vacuum degree of the evaporator. The modified mathematical model fits the experimental data of the system fairly well (deviation of less than 4.5%).
- While the concentration of feed water goes up, the performance of the system has a small increase, which does not have much influence. The PR and GOR decrease by about 5% with the 20% increase of feed water flow rate. With the increase of the feed water temperature, the PR and GOR of the system increase. The whole system is able to perform well under the feed water flow rate of 400–600 kg/h, or the inlet temperature of 60°C–90°C. Plus, the system will have a better performance if the heat insulation is enough or the TVC is led into the system.
- As for zero liquid discharge, a crystallizer can be coupled with MEE in future research. It requires further research to figure out the method of coupling as well as the appearance of the new system.

Acknowledgement

This work is supported by Science and Technology Major Project of Liaoning Province (2019) (No. 2019JH1/10300002), China.

Symbols

A	—	Heat transfer area, m^2
BPE	—	Boiling point elevation, °C
C	—	Concentration of brine, %
cp	—	Specific heat capacity at constant pressure, J/(kg°C)
CW	—	Flow rate of preheater heat source heating steam, kg/h
D	—	Secondary steam flow rate, kg/h
d	—	Pipe diameter, m
F	—	Feed water flow rate, kg/h
FW	—	Freshwater flow rate at the preheater heat source outlet, kg/h
G	—	Flow rate of liquid from the former unit, kg/h

g — Gravitational acceleration, m/s^2
K — Heat transfer coefficient, W/(m^2°C)
LTMD — Logarithm mean temperature difference, °C
NEA — Non-equilibrium allowance, °C
R — Latent heat of liquefaction, kJ/kg
r — Latent heat of vaporization (latent heat efficiency 96%), kJ/kg
T — Temperature of steam, °C
t — Temperature of liquid, °C
W — Heating steam flow rate, kg/h
Γ — Spray density, m^3/(m^2·s)
α — Heat transfer coefficient of phase change on either side of pipe, W/(m^2·°C)
δ — Thickness of pipe wall, m
η — Heat transfer efficiency, 98%, –
λ — Heat conductivity, W/(m·°C)
μ — Dynamic viscosity, Pa·s
ν — Kinematic viscosity, m^2/s
ρ — Density, kg/m^3

Subscript

c — Condensate
f — Fouling
D — Steam
i — i-th effect
in — Inlet
L — Liquid
out — Outlet
p — Preheater
w — Wall of pipe

References

[1] UNEP, Vital Water Graphics: An Overview of the State of the World's Fresh and Marine Waters, UNEP, 2008.
[2] J. Lienhard, T. Gregory, W. David, B. Leonardo, Low Carbon Desalination: Status and Research, Development, and Demonstration Needs, Cambridge, Massachusetts, n.d.
[3] C. Li, Y. Goswami, E. Stefanakos, Solar assisted sea water desalination: a review, Renewable Sustainable Energy Rev., 19 (2013) 136–163.
[4] M. Padaki, R. Surya Murali, M.S. Abdullah, N. Misdan, A. Moslehyani, M.A. Kassim, Membrane technology enhancement in oil-water separation. A review, Desalination, 357 (2015) 197–207.
[5] H. Zhang, Z. Zhong, W. Xing, Application of ceramic membranes in the treatment of oilfield-produced water: effects of polyacrylamide and inorganic salts, Desalination, 309 (2013) 84–90.
[6] M. Ebrahimi, K. Shams Ashaghi, L. Engel, D. Willershausen, P. Mund, P. Bolduan, Characterization and application of different ceramic membranes for the oil-field produced water treatment, Desalination, 245 (2009) 533–540.
[7] S.E. Weschenfelder, A.C.C. Mello, C.P. Borges, J.C. Campos, Oilfield produced water treatment by ceramic membranes: preliminary process cost estimation, Desalination, 360 (2015) 81–86.
[8] A. Mohsen, M. Mirfendereski, M. Nikbakht, M. Golshenas, T. Mohammadi, Performance study of mullite and mullite-alumina ceramic MF membranes for oily wastewaters treatment, Desalination, 259 (2010) 169–178.
[9] T. Muhammad, A.A. Mojjly, A. Al-Othman, N. Hilal, Membrane separation as a pre-treatment process for oily saline water, Desalination, 447 (2018) 182–202.
[10] A. Khalifa, H. Ahmad, M. Antar, T. Laoui, M. Khayet, Experimental and theoretical investigations on water desalination using direct contact membrane distillation, Desalination, 404 (2017) 22–34.
[11] A. de la Calle, J. Bonilla, L. Roca, P. Palenzuela, Dynamic modeling and simulation of a solar-assisted multi-effect distillation plant, Desalination, 357 (2015) 65–76.
[12] A. de la Calle, J. Bonilla, L. Roca, P. Palenzuela, Dynamic modeling and performance of the first cell of a multi-effect distillation plant, Appl. Therm. Eng., 70 (2014) 410–420.
[13] S. Azimibavil, A.J. Dehkordi, Dynamic simulation of a multi-effect distillation (MEE) process, Desalination, 392 (2016) 91–101.
[14] M. Alsehli, M. Alzahrani, J.K. Choi, A novel design for solar integrated multi-effect distillation driven by sensible heat and alternate storage tanks, Desalination, 468 (2019) 114067.
[15] I.B. Askari, M. Ameri, Techno economic feasibility analysis of Linear Fresnel solar field as thermal source of the MED/TVC desalination system, Desalination, 394 (2016) 1–17.
[16] I.B. Askari, M. Ameri, The application of linear Fresnel and parabolic trough solar fields as thermal source to produce electricity and fresh water, Desalination, 415 (2017) 90–103.
[17] I.B. Askari, M. Ameri, F. Calise, Energy, exergy and exergo-economic analysis of different water desalination technologies powered by Linear Fresnel solar field, Desalination, 425 (2018) 37–67.
[18] C. Ghenai, D. Kabakebji, I. Douba, A. Yassin, Performance analysis and optimization of hybrid multi-effect distillation adsorption desalination system powered with solar thermal energy for high salinity sea water, Energy, 215 (2021) 119212.
[19] M.L. Elsayed, O. Mesalhy, R.H. Mohammed, L.C. Chow, Transient and thermo-economic analysis of MEE-MVC desalination process, Energy, 167 (2019) 283–296.
[20] A. Farsi, I. Dincer, Development and evaluation of an integrated MED/membrane desalination system, Desalination, 463 (2019) 55–68.
[21] E. Ali, J. Orfi, H. AlAnsary, J.G. Lee, A. Alpatova, N. Ghaffour, Integration of multi effect evaporation and membrane distillation desalination processes for enhanced performance and recovery ratios, Desalination, 493 (2020) 114619.
[22] P. Guo, T. Li, P. Li, Y. Zhai, J. Li, Study on a novel spray-evaporation multi-effect distillation desalination system, Desalination, 473 (2020) 114195.
[23] G. Kosmadakis, M. Papapetrou, B. Ortega-Delgado, A. Cipollina, D.C. Alarcón-Padilla, Correlations for estimating the specific capital cost of multi-effect distillation plants considering the main design trends and operating conditions, Desalination, 447 (2018) 74–83.
[24] M. Papapetrou, G. Micale, G. Zaragoza, G. Kosmadakis, Assessment of methodologies and data used to calculate desalination costs, Desalination, 419 (2017) 8–19.
[25] B. Ortega-Delgado, P. Palenzuela, D.C. Alarón-Padilla, Parametric study of a multi-effect distillation plant with thermal vapor compression for its integration into a Rankine cycle power block, Desalination, 394 (2016) 18–29.
[26] I.S. Al-Mutaz, I. Wazeer, Development of a steady-state mathematical model for MEE-TVC desalination plants, Desalination, 351 (2014) 9–18.
[27] J.R. Thome, Engineering Data Book III, Wolverine Tube Inc, 2004.
[28] K.R. Chun, R.A. Seban, Performance prediction of falling-film evaporators, J. Heat Transfer, 94 (1972) 432–436.
[29] O. Miyatake, K. Murakami, Y. Kawata, Heat Transfer, Jpn. Res., 2 (1973) 89–100.
[30] R. Bellman, R.H. Pennington, Effects of surface tension and viscosity on Taylor instability, Q. Appl. Math.,12 (1954) 151–162.
[31] J.H. Lienhard, P.T.Y. Wong, The dominant unstable wavelength and minimum heat flux during film boiling on a horizontal cylinder, J. Heat Transfer, 86 (1964) 220–225.
[32] D. Maron-Moalem, S. Sideman, A.E. Dukler, Dripping characteristics in a horizontal tube film evaporator, Desalination, 27 (1978) 117–127.
[33] E.N. Ganic, M.N. Roppo, An experimental study of falling liquid film breakdown on a horizontal cylinder during heat transfer, J. Heat Transfer, 102 (1980) 342–346.
[34] L. Yang, S. Shen, Experimental study of falling film evaporation heat transfer outside horizontal tubes, Desalination, 220 (2008) 654–660.